Meteorol. Atmos. Phys. 79, 105–126 (2002)

Meteorology and Atmospheric Physics

© Springer-Verlag 2002
Printed in Austria

[1] Center for Climate Systems Research, Columbia University at the NASA/Goddard Institute for Space Studies New York, USA
[2] Department of Meteorology, Florida State University, Tallahassee, USA

A simple soil moisture scheme for regional climate simulations in the tropics

M. Fulakeza[1], **L. M. Druyan**[1], and **T. N. Krishnamurti**[2]

With 14 Figures

Received June 28, 2001
Revised August 27, 2001

Summary

A regional climate model (RCM) is described which incorporates an improved scheme for soil moisture availability (SMA) compared to an earlier version. The improvement introduces a sensitivity of SMA to soil type, vegetation cover and ground albedo, making the model more adaptable to divers regions. In addition, the interactive SMA depends on past precipitation, ground temperature and terrain relief. Six RCM simulations of the monthly mean climate over southern Africa are performed at 0.5° grid spacing. Improvements in the RCM climate simulations compared to control runs are attributed to the newer SMA scheme. Only a slight improvement in skill results from driving the RCM with observational analyses as opposed to GCM "predicted" lateral boundary conditions. The high spatial resolution of the RCM provides a distinct advantage in the simulated spatial distribution of precipitation compared with a global model run at an effective grid spacing of 2.8°. The mesoscale precipitation signal in the RCM simulations is more dominant during the rather dry December 1982 than during December 1988. The improved SMA scheme contributed to a realistic partition between latent and sensible heat fluxes at the ground-atmosphere boundary and consequently a realistic diurnal cycle of ground temperature. Simulated differences in the spatial distribution of rainfall between December 1982 and December 1988 are more realistic with the improved scheme.

1. Introduction

Climatic variability can be associated with secular trends, which produce changes in an average state, or with variability about a constant mean. "Regional" spatial climate variations, on the order of 50–1000 km, can sometimes be extreme, resulting in floods or droughts, such as the devastating droughts over Africa 1982/83 and 1992, and the more recent (March, 2000) floods in Mozambique. There is an extremely important socio-economic benefit in gaining a better understanding of the mechanisms related to extreme regional climate occurrences.

Both numerical and observational studies are appropriate for researching extreme climate events. In the case of numerical modeling, answers are sought through climate simulations using global general circulation models (GCMs) and regional limited area models (LAMs). Although GCMs are recognized as powerful research tools for climate studies, their typical horizontal grid spacing is too coarse to obtain meaningful results in the presence of substantial topographic relief or to provide reliable regional and local scale information. An adequate increase in GCM resolution requires large increases in computational capabilities which strain existing resources. This suggests the advantages of regional climate simulation whereby model resolution is increased in only a limited domain by nesting within coarser gridded GCMs (Giorgi, 1990). In this way GCMs' responses to global forcing terms

can be supplied to a regional climate model which in turn can provide detailed climatic patterns over the limited area.

Anthes et al. (1989) investigated the climatological skill of the Pennsylvania State University/ National Center for Atmospheric Research (PSU/ NCAR) mesoscale model (MM4). In their study, 12 different synoptic cases over the eastern United States were simulated and analyzed with the MM4 driven by different observed initial and lateral boundary conditions. Objective skill scores over the ensemble were quite good, but the performance of the model for individual cases varied considerably. Another important conclusion from this study was that the lateral boundary conditions (LBCs) exerted much stronger control over the error growth than the initial conditions or the use of different physical parameterizations. This characteristic may be more valid for midlatitude simulations than for tropical ones.

Monthlong simulations with the MM4 driven by analyses of observations and NCAR Community Climate Model (CCM) fields were carried out by Giorgi and Bates (1989), Giorgi (1990), and Giorgi (1991). These were the first simulations in which a LAM was run for a month without being reinitialized. The output from these long runs demonstrated how the use of a LAM improves the simulation of the regional distribution of surface climatic variables over areas of complex terrain compared to the use of coarse-scale GCMs alone. Giorgi et al. (1993) conducted 3.5-year-long MM4 climate simulations over the continental United States, one for present-day conditions and one for conditions under double carbon dioxide concentration. Although results showed realistic features, in some respects more realistic than the coarse resolution driving model, the control simulation also indicated significant differences from observed present-day climatology over the region. Much of this error arose from the poor quality of lateral boundary conditions provided by the CCM. Unlike previous studies, the model reproduced quite well the observed surface climatology when driven by analyses of meteorological fields (Giorgi et al., 1993).

Giorgi and Marinucci (1996) showed examples of weather events that were simulated by a LAM with better than persistence skill even weeks to months after the initial conditions. In such circumstances, the model's generation of actual climate features is made possible by the combination of model physics and observed meteorological information entering at the lateral boundaries (Giorgi and Mearns, 1999).

Sun et al. (1999a) found it prudent to customize the NCAR Regional Climate Model (RegCM2) by tuning it to the observed October climate before they applied it to the simulation of interannual climate variability. Sun et al. (1999b) ran the RegCM2 on a 60-km grid to study the short rains of East Africa. Simulations spanned four months (September–December) for each of 12 years and were initialized and forced (via lateral boundary conditions) from ECMWF reanalysis data. The simulated interannual variability of precipitation was favorably validated against observations for several sub-regions and, owing to the high resolution, composites of wet and dry years showed notable differences in circulation mechanisms. The paper discussed how ENSO and synoptic features of the large-scale circulation are related to simulated precipitation anomalies, but did not consider how the model's high horizontal resolution may have improved the analysis of near-surface circulation and temperature compared to the coarser gridded ECMWF data that was driving the model. It also did not analyze the role of soil moisture in the interannual climate variability.

The regional model's ability to perform well over long-term continuous simulations not only depends on the aforementioned initial and lateral boundary conditions but also on how it allows interactive coupling with surface physics, the ecosystem, and ground hydrology. In order to properly parameterize surface fluxes in the MM4, the Biosphere-Atmosphere Transfer Scheme (BATS) (Dickinson et al., 1986) was used for the surface physics/ soil hydrology calculations. The BATS is a model of land surface processes designed to describe the role of vegetation and interactive soil moisture in modifying the surface fluxes of momentum, heat, and moisture. However, sensitivity studies (Sellers and Dorman, 1987) have shown that errors in the specification of certain properties associated with land surface processes could lead to uncertainties on the order of 7% in the net radiation estimates and up to 25% in the calculation of evapotranspiration flux. It has been suggested (Bounoua, 1992) that similar discrepancies are obtained by using simpler

parameterizations utilizing many fewer parameters. Additionally, a comparison of the computer time necessary to run a two surface parameterization in a one dimensional model showed that the biophysically based scheme requires about 43% more time than the conventional one. Accordingly, a computer efficient scheme for estimating surface evapotranspiration that has a robust beneficial impact on climate simulations has appeal.

A number of land surface process schemes for climate simulation and numerical weather prediction have been developed. Although BATS is quite sophisticated, it nevertheless did not include any influences of terrain elevation or slope on soil moisture characteristics. A parameterization of land surface processes that did account for terrain relief was developed at the Florida State University (Dastoor and Krishnamurti, 1991; Bounoua, 1992). This scheme for keeping track of soil moisture availability (SMA) was based on a vertically integrated soil moisture budget. SMA, expressed as a percent of saturation, was made a function of past rainfall, albedo, surface temperature and terrain slope in order to account for the responses of both soil morphology and the climate forcings. A wide range of land surface types (India and adjacent regions) were considered in the development of the SMA predictive equation. However, no attempt was made to vary the relationship according to vegetation and soil type which influence the modulation of fluxes of momentum, heat and moisture. In addition, in the previous scheme, while surface temperature and rainfall were updated during model integration, albedo remained constant.

Theoretical studies on the relationship between vegetation and rainfall over Africa have made use of the Normalized Difference Vegetation Index (NDVI). The relationship between NDVI and rainfall has been studied in a series of papers (Malo and Nicholson, 1990; Nicholson et al., 1990; Davenport and Nicholson, 1993). The studies show a clear linear relationship between annually integrated NDVI and mean annual rainfall and, further, that their spatial patterns are similar over the Sahel region of West Africa. This relationship becomes uncertain, however, regarding the intraseasonal variability of NDVI. In East Africa, unlike in the Sahel, the relationship is more log-linear. As rainfall increases, NDVI slowly increases until it asymptotes at a constant threshold value. The situation is similar for southern Africa but the threshold there appears to be lower. There appears to be a positive relationship in relatively dry locations between annual and monthly mean rainfall and NDVI below thresholds for saturation, while in humid regions, the NDVI approaches a constant value as rainfall continues to increase. It was also found that the NDVI/ rainfall relationship is vegetation and soil type specific.

Using a climatology model with no dynamics or physics, Lare (1992) investigated the relative roles of large-scale phenomena versus land surface-atmosphere feedbacks in the initiation and perpetuation of drought over the Sahel and Kalahari in Southern Africa. This model uses incoming solar radiation and observed precipitation, then calculates ground- absorbed solar radiation, evapotranspiration, soil moisture, runoff, energy balance fluxes, and atmospheric temperatures. The results showed that in southern Africa NDVI patterns reflected soil moisture tendencies at all locations, but they also correlated well with evapotranspiration, particularly in wetter regions. In the wetter regions, Lare (1992) found no discernible relationship between NDVI and rainfall patterns, suggesting that other local factors such as soil type and terrain may play significant roles. By including these local factors in high resolution models having full dynamics and physics, NDVI may be used to prescribe soil moisture availability over southern Africa.

With the deficiencies of earlier schemes noted, an efficient but adequate scheme is proposed here for use in a LAM. It is based on Dastoor and Krishnamurti (1991) and Bounoua (1992) but it accounts for variegated vegetation, soil type and albedo. The improved algorithm was included in the LAM at the Florida State University where the model was tested in a series of monthly runs over southern Africa (south of 5° S) by Fulakeza (1998). The present study demonstrates that the newly applied sensitivity to vegetation has a beneficial impact on simulated rainfall via the modification of soil moisture availability (SMA) and sensible and latent heat fluxes. In the experiments described below, data from a GCM and from ECMWF gridded analyses convey information to the regional model in order to represent the influence of large scale circulation and global forcings.

2. Model description

2.1 Overview

The LAM described here was developed at Florida State University (FSU) and was more recently applied to additional regional climate studies at the Center for Climate Systems Research (CCSR) of Columbia University, sharing facilities with the NASA/Goddard Institute for Space Studies (GISS). This LAM will hereafter be referred to as the CCSR/GISS Regional Climate Model (RCM). A detailed description of its predecessor can be found in Kumar (1989), and Krishnamurti et al. (1990). The RCM has been previously used to study African wave disturbances (Druyan et al., 2000, 2001). It has the same basic structure as the FSU global spectral model except it is a grid point model. It uses the primitive equations with a semi-Lagrangian advection scheme and semi-implicit time differencing at 15 vertical sigma levels. An Arakawa C grid (Arakawa and Lamb, 1977) is used for the horizontal staggering. In addition, the model includes the parameterization of deep cumulus convection, based on Kuo (1965, 1974), but modified by Krishnamurti et al. (1983). Other parameterizations of physical processes are described in detail in Krishnamurti et al. (1990), hence only a brief description of each of them, including recent modifications, is discussed here.

2.2 Parameterization of deep cumulus convection

The CCSR/GISS RCM computes deep convection using a modification by Krishnamurti et al. (1983, 1990). According to the original formulation, moistening and heating by the convective cloud are proportional to the humidity and temperature differences between the cloud and its environment. The proportion of the available heat and moisture supply that is assumed to be added to the column by cumulus convection must be assigned. To improve the match between simulated and observed rainfall, Krishnamurti et al. (1983, 1990) introduced mesoscale moisture convergence and moistening parameters. The mesoscale convergence is regarded as non-measurable and sub-grid scale. In the modified scheme the parameterization determines the moisture convergence and moistening parameters from knowledge of large scale variables. Krishnamurti et al. (1983, 1990) showed that the large-scale vertically integrated vertical velocity and lower troposphere (700 hPa) relative vorticity can serve as successful proxies for the mesoscale moisture convergence and moistening parameters in the modified Kuo scheme.

2.3 Lateral boundary conditions (LBCs)

LBCs for regional modeling present a challenge, since the RCM requires climate information about the region outside its domain. A number of pragmatic approaches to integrating LBC have been developed over the years (Krishnamurti et al., 1990) and an excellent review is given by Davies (1983). The most frequently used methods can broadly be grouped into 2 categories, (i) one way grid nesting, in which a model integrated over a larger domain is used to specify LBCs for the smaller domain (Chen and Miyakoda, 1974; Miyakoda and Rosati, 1977; Leslie et al., 1981), and (ii) the formulation of open LBCs that allow disturbances to radiate out of the model domain with minimum boundary reflections.

In the experiments described here, LBCs are obtained from either the FSU global spectral model (FSUSM) or ECMWF observational analyses. These externally specified field values are then merged with forecasted variables produced by the RCM by weighting them with progressively decreasing weights inward within a buffer zone that completely surrounds the domain of interest. Optimal treatment of this approach avoids over-damping of incoming waves, but care must also be taken not to create reflections by too sharp a transition. The buffer zone consists of n grid elements and the relative weights [wt] of the LBCs vary according to the formulation:

$$\mathrm{wt} = k^* \exp(-p^* r), \tag{1}$$

where k and p are coefficients that determine the relative influence of the LBCs and r is the row number from 1 to n. For the present simulations the buffer zone consists of six grid elements ($n = 6$), $k = 2.2$, and $p = 0.8$.

2.4 Formulation of soil moisture availability

The interaction between the atmosphere, land surface, and the biosphere plays an important role in

determining climate evolution through exchanges of radiation, heat, moisture, and momentum. It is evident from climate data analyses and model experiments that the atmosphere is sensitive to variations in land surface processes, and especially to the soil moisture (Dastoor and Krishnamurti, 1991). Increases in soil moisture lead to increased evapotranspiration from the land surface which may enhance local rainfall while desiccation inhibits rainfall. In addition, evapotranspiration limits ground temperature increases by removing latent heat.

The most recent modifications to the CCSR/GISS RCM relate to the formulation of soil moisture availability (SMA). SMA is defined as the ratio of soil moisture at the surface to a maximum saturation value (field capacity) for a given soil type at a given grid element. Evapotranspiration is modeled as the product of the SMA and the potential evapotranspiration.

Earlier numerical model studies made many simplifications in order to parameterize SMA. The SMA experiments reviewed by Mintz (1984) lacked geographical variations of most surface characteristics. More complex schemes which include geographic variations of albedo, roughness length, and root depth have since been developed (Dickinson et al., 1986; Sellers et al., 1986; Rosenzweig and Abramopoulos, 1997).

SMA is part of the total liquid moisture budget whose components are precipitation, surface runoff, snow melt and infiltration and it depends on soil and vegetation types. Since the interaction among these processes is complex for a typically heterogeneous grid element, explicit prediction of SMA is challenging. The situation is especially cumbersome when vegetation is considered.

The basis of the present soil moisture parameterization overcomes some of the difficulties of deterministic computation of SMA. It was originally developed by Dastoor and Krishnamurti (1991) and improved by Bounoua (1992). In this approach, SMA values (estimated for a range of conditions) are expressed as a multivariate function of past rainfall, surface temperature, and terrain relief in order to account for the response of climate forcing. The functions are obtained by regression analysis relating estimates of SMA with observations of those variables. While this approach is considerably less complex than physically-based land surface models, it is computer efficient and provides realistic variability of surface energy fluxes (see below).

The procedure for computing the preliminary SMA distributions for the regression analysis is based on moisture continuity considerations and is explained in detail in Dastoor and Krishnamurti (1991).

In the current version of the RCM (Fulakeza, 1998; Druyan et al., 2000, 2001), SMA multivariate functions are derived by relating SMA as before to past rainfall, surface temperature and terrain relief. The latest improvement is achieved by adding dependence on albedo and Normalized Difference Vegetation Index (NDVI, from radiometric data observed by NOAA satellites). This additional sensitivity to land surface characteristics is particularly suitable for simulations over Africa. The current SMA dependence on the interaction of these variables is expressed by using a selective second-order regression scheme. In addition, a unique multivariate regression is developed this way for each of several sub-regions of uniform soil type over the entire domain. It should be noted that 5-day past rainfall has been used because soil moisture strongly depends on the most recent rainfall (Bounoua, 1992). Gash et al. (1992) showed that evaporation remains quite close to its potential for about a week after the last occurrence of rain for most types of terrain.

The terrain and albedo variables used in the regression analysis are dimensionless, defined by:

$$x_{ij} = (X_{max} - X_{ij})/(X_{max} - X_{min}), \qquad (2)$$

where X is either the albedo or the terrain elevation and the subscripts refer to the local grid point (ij) and the maximum and minimum values over the entire domain.

By prescribing observed values of NDVI it is possible to investigate the effect of vegetation on soil moisture availability and consequently on surface latent heat fluxes. NDVI uses reflectance data (Watts m^{-2}) in the visible (CH1: 0.58 to 0.68 μm) and near infrared (CH2: 0.73 to 1.10 μm) bands. It is the main global vegetation index product produced by NOAA/NESDIS since the latter part of 1983. NDVI is defined as

$$\mathrm{NDVI} = (\mathrm{CH2} - \mathrm{CH1})/(\mathrm{CH2} + \mathrm{CH1}). \qquad (3)$$

NDVI is a measure of the plant surface chlorophyll density and increases as the density in

vegetation cover increases. It generally ranges between 0.0 (i.e., no vegetation) and 0.6 (dense vegetation). The NDVI is sensitive to water vapor, aerosols, clouds, off-nadir viewing, varying sun angle (Justice et al., 1985; Tucker and Sellers, 1986), and soil type. Water vapor tends to lower NDVI values by decreasing the near infrared reflectance. To reduce the effect of atmospheric attenuation and sensitivities, a composite method is used in the new scheme such that maximum values observed in a given month are assumed to be representative of the true vegetative conditions for the month (Lare, 1992). However, bi-weekly NDVI data can be utilized during model integrations by applying a time smoothing to any variations that occur within the two weeks for which the data are provided.

Figure 1 shows bi-weekly NDVI for December 1988. There is significant difference in the spatial distribution of NDVI between the first and second two-week periods. Higher values (Fig. 1a) eventually give way to lower indices (Fig. 1b), implying a negative trend in the greenness of vegetation between the first and the last two weeks of December 1988.

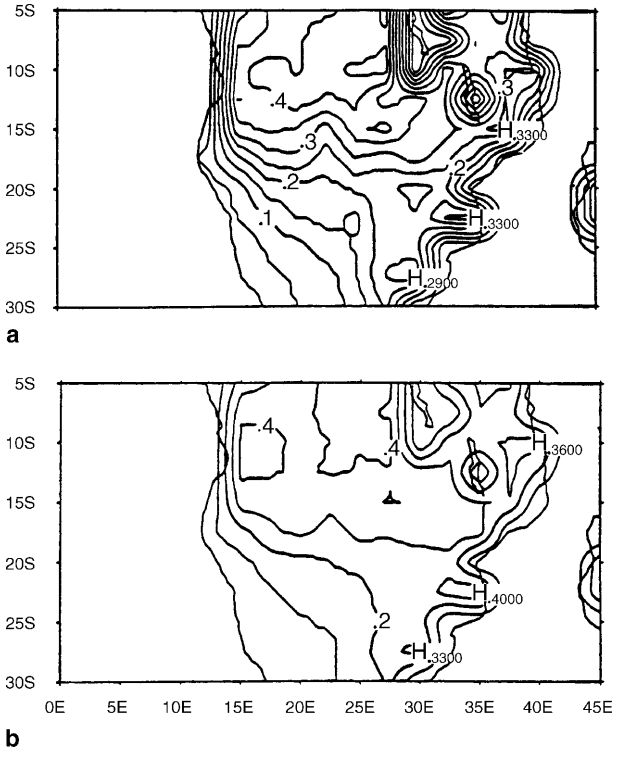

Fig. 1. Normalized Difference Vegetation Index (NDVI). **a** for December 1–15, 1988; **b** for December 16–31, 1988. Dimensionless values are resolved for 0.5° grid elements

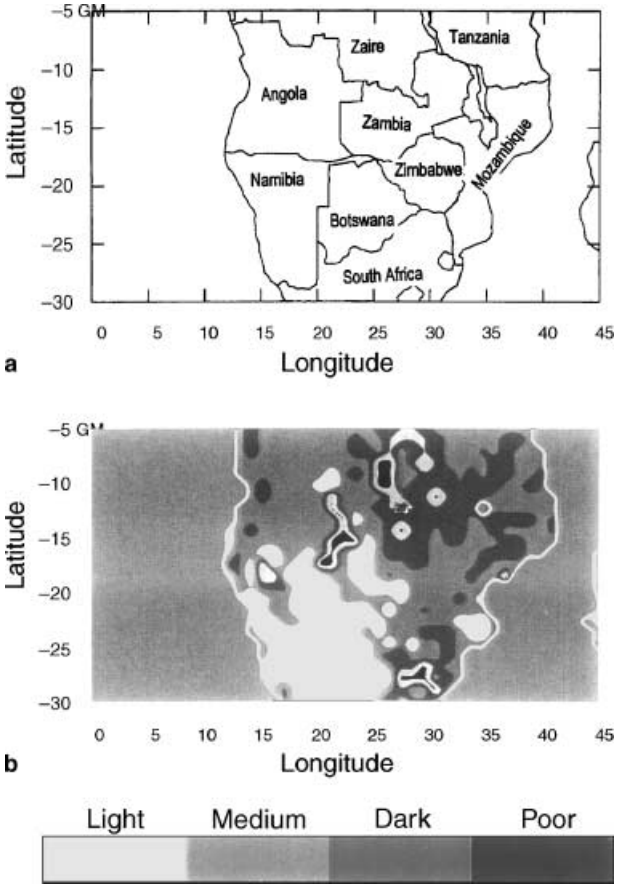

Fig. 2a. Domain for model simulations showing the national boundaries; **b** Soil colors. The designation ''poor'' represents light, medium and dark soils having poor drainage. A single regression for SMA was derived for the combined dark and poor areas. Data is gridded for 1° elements

In order to optimize the number of predictors, a screening method was applied. The southern Africa domain (Fig. 2a) was divided into subregions according to the soil classifications of Wilson and Henderson-Sellers (1985) and the multivariate analysis was done in each subregion. The data comprised categories of color: light, medium, and dark; texture: coarse, intermediate and fine and drainage: free, impeded, or poor. These data are available at a resolution of 1 degree latitude by 1 degree longitude and were interpolated to the model's grid at a resolution of 0.5° (Fig. 2b). In each sub-region, several regressions were tested with a varying number of predictors. The tests showed that a significant amount of variance is explained by only nine variables, and only three distinctly different regression relationships emerged from the analysis for the five subregions of southern Africa that were examined.

Table 1. Regression coefficients used by the RCM to compute SMA (%) for each of three soil types during December 1988 in southern Africa. Data were combined from dark soil and poorly drained soil sub-regions. The square value of temperature did not explain any SMA variance

Variable	Coefficient	Light soil	Medium soil	Dark soil
constant	a_0	3.6691	2.8223	2.3180
precipitation ($mm\,d^{-1}$)	a_1	0.6047	0.5925	0.4841
temperature (°K)	a_2	−0.0116	−0.0086	−0.0126
albedo	a_3	0.1905	0.1441	0.1361
terrain relief	a_4	0.2716	0.2668	0.2903
NDVI	a_5	0.6770	0.3317	0.3242
precipitation^2 ($mm\,d^{-1}$)^2	a_{11}	−0.1900	−0.1852	−0.1898
albedo^2	a_{33}	−0.0894	0.0287	−0.1080
(terrain relief)^2	a_{44}	−0.0039	−0.0406	0.0104
NDVI^2	a_{55}	−0.4107	0.1019	−0.3854

Regression results did not make a significant distinction between soil texture and drainage types, only soil color. The nine chosen predictors were then regressed against the estimates of SMA for each color type and the resulting regression coefficients are given in Table 1. Note that ''dark soil'' also includes data from the small areas designated ''poor drainage'' in Fig. 2b.

The selected coefficients reflect the sensitivity of SMA to each variable. The coefficients for temperature are small because the variable, in the order of 300° K, takes on larger values than the normalized albedo or terrain which are always ≤ 1.0. The negative coefficients for temperature indicate that SMA tends to be lower at higher temperatures, all other things being equal. Positive coefficients for the other variables mean that SMA increases for rainier, darker conditions and for more dense vegetation coverage. In addition, low terrain elevations tend to have higher SMA (see Eq. (2)).

The derived regression equations are used by the RCM to update SMA during model simulations, using modeled rainfall, surface temperature, terrain relief and albedo as the independent variables. Land surface albedo is computed as a function of moisture availability during the integration of the model using the formulation by Deardorff [1978]:

$$\text{albedo} = 0.31 - 0.17^{*}SMA. \quad (3)$$

Future experiments will test the advantages of introducing albedo dependence on soil type.

3. Experiments

We discuss the results of six one-month simulations over southern Africa with the RCM, two for December 1982, one for February 1983 and three for December 1988.

Table 2 summarizes the design of each experiment. In five of the monthly simulations, LBCs came from the FSU global spectral model (FSUSM) simulations forced with observed SST at an effective resolution of 2.8°, while the sixth was forced with data from ECMWF global analyses on a 2.5° grid. Four of the simulations used the newer multivariate scheme for SMA described above (Fulakeza, 1998; Druyan et al., 2000, 2001), while the two control runs for exp1 and exp4 (exp2 and exp5, respectively) were made using the earlier regression equations for SMA, as in Bounoua (1992). This original SMA formulation, based on climate data over India, did not include NDVI or albedo as independent variables. Moreover, SMA was computed by a single function for all soil types. Comparison of exp1 and exp4 results to their controls (exp2 and exp5, respectively) therefore tests the sensitivity of the RCM simulated monthly mean climate over southern Africa to SMA that accounts for land surface heterogeneity. Exp3 is compared with exp1 to evaluate how well the RCM responds to seasonality, changed initial conditions and different LBC. Note that the initial conditions for exp3 on February 1, 1983 were taken from a continuous FSUSM integration so that, in contrast to the other four experiments, the simulation did not start with the observed atmospheric state. The simulation forced with ECMWF for December 1988 (exp6) shows the relative benefits of observed LBC data in contrast to FSUSM forcing (exp4). In the presentation of results below, RCM monthly mean climate fields are also compared with corresponding FSUSM

Table 2. Description of the six one-month RCM simulations analyzed in the study

	Month	Initial conditions and LBC	Soil moisture availability
1.	Dec'82	FSU global spectral model	current version
2.	Dec'82	FSU global spectral model	former version
3.	Feb'83	FSU global spectral model	current version
4.	Dec'88	FSU global spectral model	current version
5.	Dec'88	FSU global spectral model	former version
6.	Dec'88	ECMWF analyses	current version

simulated fields as well as with observational evidence.

Studies on seasonal time scales based on the FSUSM include Krishnamurti et al. (1989); Fulakeza (1991); Bounoua (1992); Krishnamurti et al. (1994); Krishnamurti et al. (1995). Evaluations indicate that the FSUSM produces monthly mean fields that generally compare well with ECMWF gridded analyses.

In addition to the initial and boundary conditions from the FSUSM or ECMWF, the RCM requires initial surface albedo, ten-day mean SST, terrain topography, NDVI, and soil type as its input. In the experiments described here, the initial surface albedo is based on Kondratyev (1972), and Posey and Clapp (1964) data for austral summer. The sea surface temperature (SST) is based on ten-day Reynolds SST values obtained from NCEP and described by Reynolds and Smith (1994). The model topography is derived from a high resolution (10×10 minute) latitude-longitude terrain field compiled by the U.S. Navy. Model terrain elevations were computed as the mean of the high resolution terrain within each half degree square. Bi-weekly observed NDVI data from NOAA/NESDIS were obtained for the December 1988 case considered here and a time smoothing was applied to remove a fifteen-day oscillation, providing mean values for each two-week period.

4. Results

4.1 December 1982 results (exp1, exp2)

Satellite observed NDVI became available only during the latter part of 1983, so actual values could not be used in this example or for February 1983. Accordingly, the SMA functions for these case studies use multi-year mean December and February NDVI values observed during subsequent years over southern Africa.

4.1.1 Sensible and latent heat flux

We evaluated the impact of the new SMA scheme on the simulation for December 1982 by first comparing the time series of sensible and latent heat fluxes (SHF, LHF, respectively) and ground temperature from exp1 to the control (exp 2) results. Time series have been constructed for

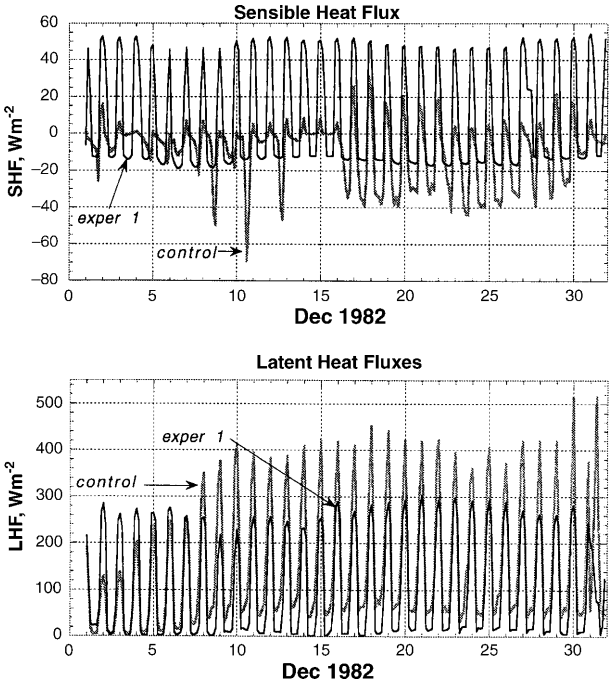

Fig. 3. Hourly sensible (top) and latent (bottom) heat fluxes at ground surface averaged over all land points for exp1 and exp2 (control) during December 1982

the entire domain average (Fig. 3) and also for each of three sub-regions (not shown) corresponding to the three soil types for which SMA functions were derived (Table 1). Ideally, one would like to compare model-derived SHF and LHF with observed values, but such observations are not available. There is a remarkable difference in the partitioning of domain-averaged SHF and LHF between the two experiments which suggests a positive impact from the SMA dependence on vegetation and soil type. Results for the entire domain shown in Fig. 3a illustrate this point. Control SHF daily maxima (mostly $<10\,\mathrm{W\,m^{-2}}$) and minima are both lower than for exp1, where the minima reflect the considerable overnight cooling. The SHF in exp1, on the other hand, peaks at about $50\,\mathrm{W\,m^{-2}}$, which is in better agreement with Budyko (1986) and, for example, with estimates of mean monthly SHFs for Bulawayo (Zimbabwe) by Lare (1992) based on a one-dimensional model. We will show that the higher and more realistic SHF of exp1 are consistent with lower evaporation rates which in turn resulted from lower (drier) SMA.

The difference in the diurnal variation of the two SHF diagrams in Fig. 3a is striking. Considerable irregularity in the control's diurnal

variations is evident while the exp1 time series has a pronounced and smooth diurnal cycle with a relatively large diurnal range. It is apparent that excessive SMA in the control limited daytime heating of ground temperatures through evaporational cooling thereby inhibiting upward SHFs.

Figure 3b shows time series of LHF averaged for the entire domain. The control run LHFs begin with reasonable values early in the month, but they increase sharply after seven days in tandem with the onset of large negative SHF. A different response is found in exp1 where SHF and LHF are more reasonably partitioned. Exp1 results show fairly uniform diurnal cycles of LHF with maxima around $250\,W\,m^{-2}$ in sharp contrast to maximum LHFs near $400\,W\,m^{-2}$ in the control experiment. Similar results were obtained individually for each of the three soil type subregions. Since the ground surface was not warming excessively (see below), a considerable portion of the incoming energy in the control must have gone into evaporating moisture. Accordingly, the control experiment produced large LHFs as a direct consequence of excessive SMA.

Ogallo (1987) reported that rainfall over southern Africa was below normal during the December 1982–February 1983 period. The Monthly Climatic Data for the World (1982, 1983) informs that many of the stations located within the domain did indeed experience rainfall deficits. Precipitation rates simulated for these experiments are discussed below in Sect. 4.3. We expect that the deficient rainfall during December 1982 would be associated with low surface LHFs, and as a result of the greater frequency of clear daytime skies, also relatively high daytime SHF. The results shown in Fig. 3a,b imply that exp1 has simulated a more reasonable variability of SHF and LHF.

4.1.2 Ground temperature

The RCM solves for ground temperature (TG) from the heat energy balance equation. The most unrealistic characteristics of the control temperatures concern the abbreviated diurnal range of TG compared to real atmospheric conditions and compared to exp1. While this is true for each of the three sub-regions, it is most pronounced for dark soils (Fig. 4) where the diurnal variation is only about 3° K for much of the month. According to climatological data for December (Torrance, 1972), the atmospheric diurnal surface air temperature range in our study region varies between 10–15° K depending on characteristics of each location, and the range of TG should be even greater. Over light-colored soil, the exp1 maximum TG is about 304° K (31 °C), which compares reasonably well with Lare's (1992) reported daytime TG for Botswana, ranging from 299–303° K (26–30 °C). As previously mentioned, the control fails to generate high daytime TG because the excessive SMA allows too much energy to be channeled into latent heat fluxes.

4.1.3 Precipitation

The precipitation feature of greatest interest over the domain is the maximum associated with the ITCZ. This convergence zone is a consequence of thermally driven circulation associated with surface heating and its position over southern Africa migrates seasonally.

Figure 5a–d shows the accumulated rainfall for December 1982 for exp1, observations, exp2 (control) and the FSUSM, respectively. The Climate Prediction Center Merged Analysis of Precipitation (CMAP; Xie and Arkin, 1997) is based on a blend of rain gauge measurements and satellite data that have been gridded at 2.5°, so this field is smoother and lacking in small-scale features compared to the more detailed rainfall pattern of model fields computed on the 50-km grid. In exp1 (Fig. 5a), the axis of maximum rainfall (ITCZ) runs from southeast to northwest across Mozambique–Zambia–Zaire with a secondary maximum through Angola near 15° S. This distribution agrees reasonably well with the observed analysis (Fig. 5b), except over the extreme northeast since the exp1 simulated ITCZ across Lake Malawi is displaced southward of the analyzed position.

As previously recalled, southern Africa experienced drought during December 1982. Except for the northern part of Zambia and Malawi, many areas experienced negative rainfall anomalies (Ogallo, 1987). We note that the very low simulated precipitation rates for exp1 over Zimbabwe and coastal Mozambique are indeed representative of the anomalously dry conditions analyzed in Fig. 5b. Lacking a multi-year model climatology,

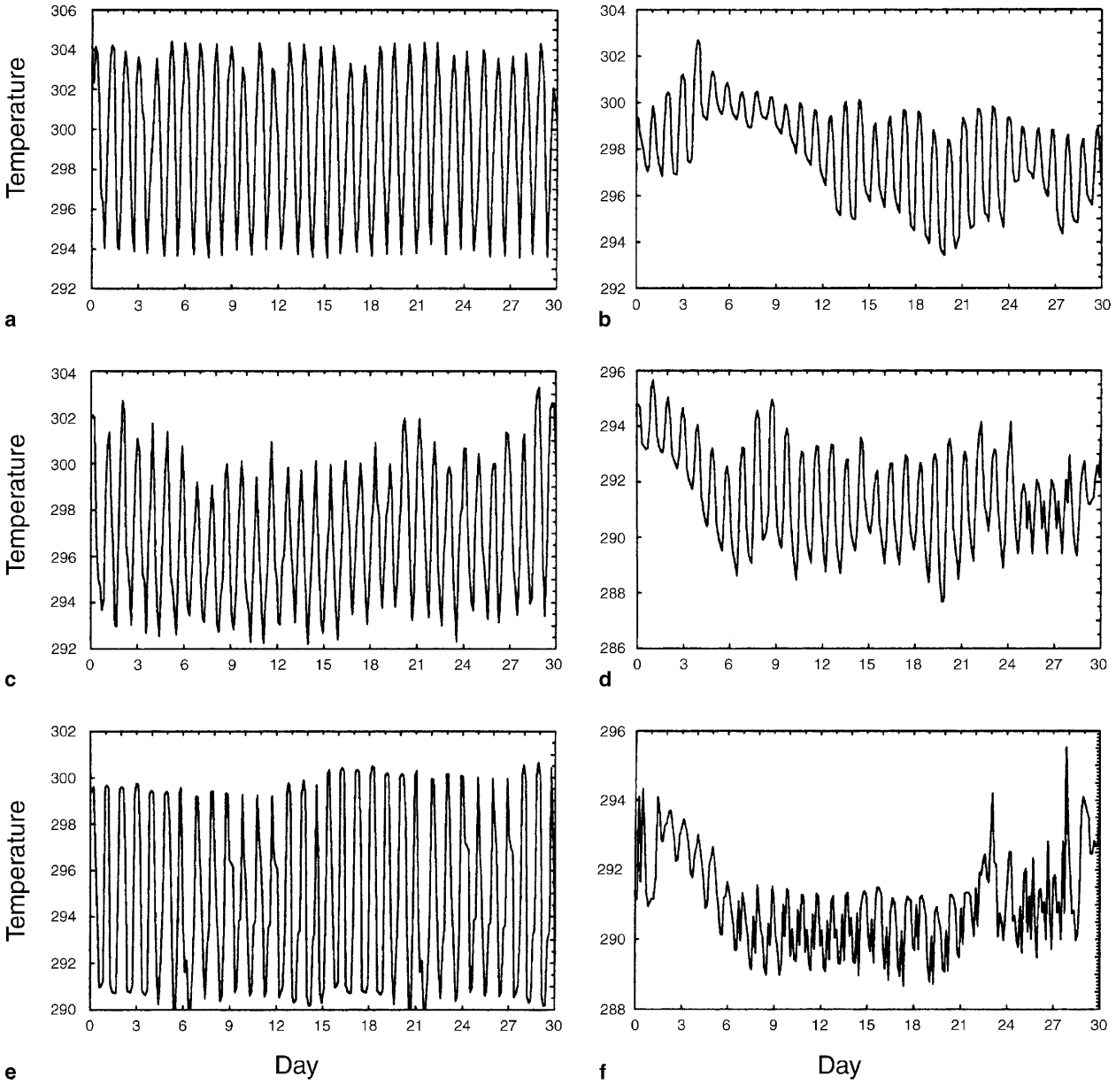

Fig. 4. Hourly ground temperatures (°K) simulated by exp1 and exp2 over each of the three soil types: **a** exp1, light, **b** exp2, light, **c** exp1, medium, **d** exp2, medium, **e** exp1, dark, **f** exp2, dark

it is not yet possible to compute simulated anomalies.

Figure 5c shows that the control run generated very large orographic maxima, no doubt related to excessively high ambient humidities, separated by wide areas of low or zero rates. It is apparent that the failure to generate high afternoon TG maxima has inhibited deep moist convection so that heavy precipitation in the control simulation has been confined to the windward slopes of steep terrain. Figure 5d shows that, by displacing the ITCZ precipitation maximum westward and by simulating no precipitation over southern Zambia, the FSUSM was also much less realistic than exp1. Heavy FSUSM rainfalls over the southeast also do not correspond with observational evidence.

Figure 6 offers a quantitative validation of exp1 versus control rainfall rates for each of the three sub-regions (soil types). The RCM with interactive SMA dependent on NDVI, albedo and soil types outperforms the control in all subregions. The exp1 advantage is greatest over dark soil and only marginally better over light soil. These

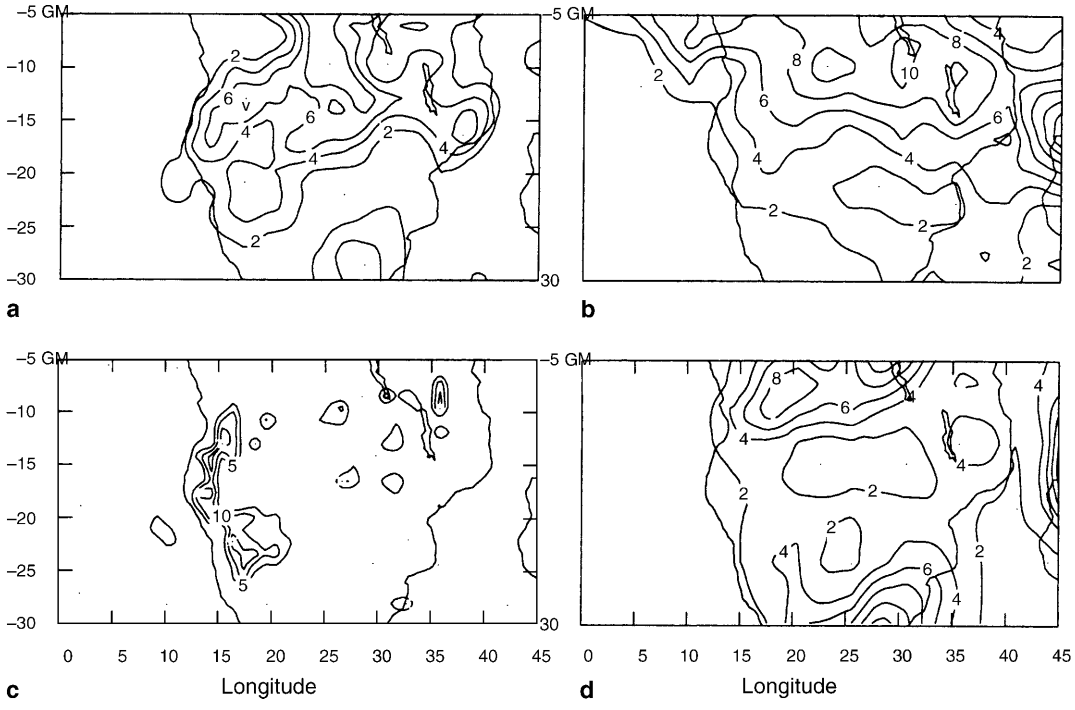

Fig. 5. December 1982 precipitation rates (mm day^{-1}). **a** exp1, **b** observed CMAP (courtesy CPC, NOAA), **c** exp2, **d** FSUSM. Data for exp1 and exp2 are represented at 0.5° grid elements, for CMAP, 2.5° grid elements and for FSUSM, 3° grid elements

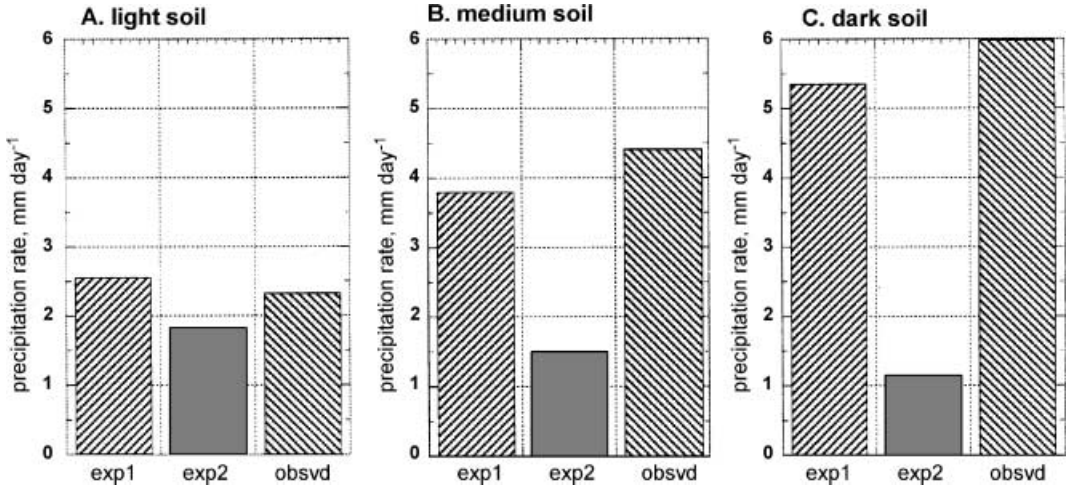

Fig. 6. Histogram of December 1982 rainfall rates averaged over each of three soil types for exp1, exp2 and observed CMAP (observations, courtesy CPC, NOAA)

results are probably more related to the topography of each subregion than the soil type since the control (exp2) simulation allowed heavy precipitation mostly along windward slopes of steep terrain (Fig. 5c). However, it is also noteworthy that the largest impact (between exp1 and control) of the newer SMA scheme on precipitation rates occurs in the dark soil areas where the impact of exp1 on daily maximum TG was the most impressive (Fig. 4). This reinforces the conclusion that the abbreviated diurnal range of TG in the control inhibited moist convective rainfall.

4.1.4 Circulation

During austral summer, one of the Southern Hemisphere's major centers of convection is located over southern Africa. It is then that southern Africa experiences the confluence of the northeast and southeast trades and the Congo air mass, forming the continental segment of the ITCZ. The convergence of these air masses leads to deep convective activity which results in widespread rainfall and localized heavy thunderstorms. Any shift in position or weakening of the ITCZ may result in a reduction of rainfall over the region.

Streamlines for the 1000 and 850 hPa circulation are plotted for exp1, control, and ECMWF observed fields in Fig. 7. Prominent features of the observed 1000 hPa circulation are the southeast trades along the southeast coast and northeasterlies over northern Mozambique and Tanzania. Exp1 streamlines represent the southeasterly trades much better than the control, while exp1 northeasterlies do not extend far enough southward. One consequence is that the confluence south of Lake Malawi is displaced slightly northward in exp1. Note, however, that this feature is completely absent in the control. Of course, the presence of high topography requires extrapolation to the 1000 hPa level and this compromises the evaluation over high terrain.

Many of the 1000 hPa features have counterparts at 850 hPa (Fig. 7d–f), for example the confluence of southeasterlies and northeasterlies south of Lake Malawi which is missed by the

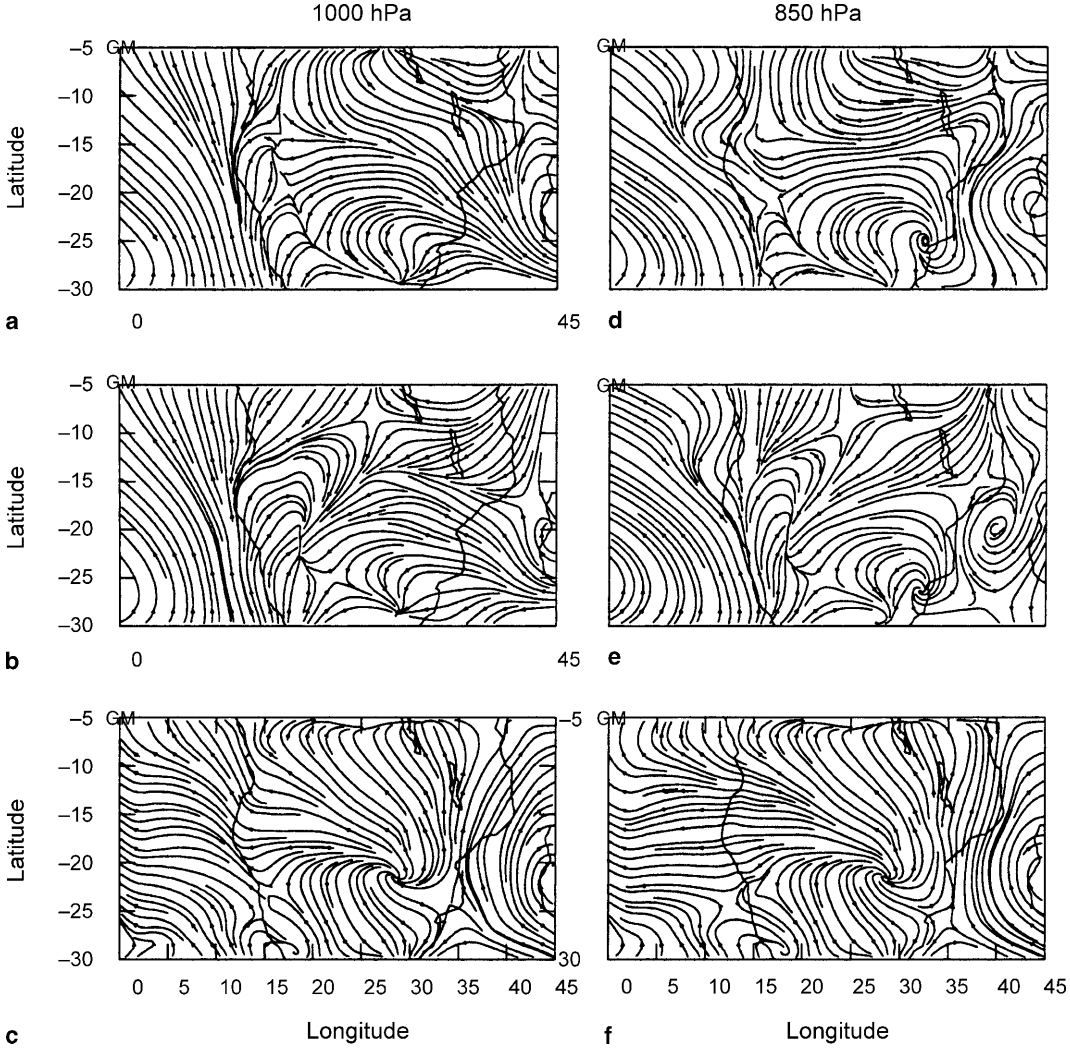

Fig. 7. Circulation of December 1982: streamflow of resultant winds at **a** 1000 hPa for exp1; **b** 1000 hPa for ECMWF; **c** 1000 hPa for exp2; **d** 850 hPa for exp1; **e** 850 hPa for ECMWF; **f** 850 hPa for exp2

control. Consequently, easterly circulation which exp1 correctly assigns to Tanzania, Malawi and Zambia, is replaced by southerlies in the control. The observational analysis (Fig. 7e) over the southeast coast shows a prominent 850 hPa ridge in juxtaposition to a cyclonic gyre over the Mozambique Channel. Although the control is able to produce a well-marked ridge, it is displaced as is the cyclonic feature. Exp1 also gives a more realistic placement of the mid-tropospheric subtropical ridge over South Africa (not shown).

4.2 February 1983 results (Exp3)

Exp3 demonstrates the sensitivity of the RCM to the initialization data, LBCs and seasonality. The model was initialized with February 1, 1983 fields from an FSUSM 2-month simulation, that are presumably not representative of the actual atmosphere on that date. Anthes et al. (1989) found that regional model simulations were less sensitive to initial conditions than to lateral boundary conditions, although their model was integrated for only 72 hr.

4.2.1 Circulation for February 1983

Figure 8 shows 1000 and 850 hPa streamlines for exp3, the corresponding observed analysis, and the FSUSM monthly mean field. Compared with December 1982 (Fig. 7), the ITCZ convergence is much sharper and cyclonic circulation dominates

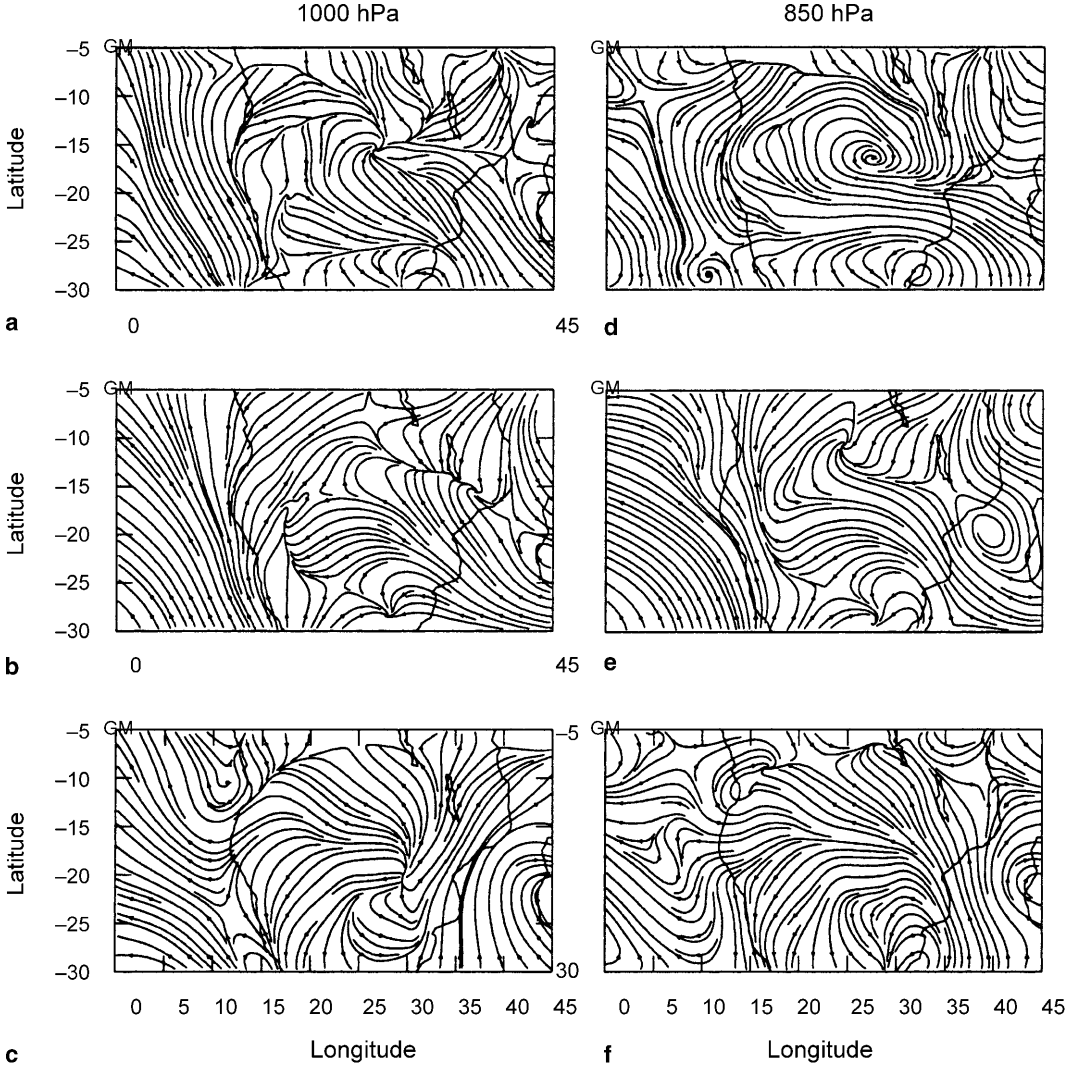

Fig. 8. Circulation of February 1983: streamflow of resultant winds at **a** 1000 hPa for exp3; **b** 1000 hPa for ECMWF; **c** 1000 hPa for FSUSM; **d** 850 hPa for exp3; **e** 850 hPa for ECMWF; **f** 850 hPa for FSUSM

the northern half of the domain corresponding to the position of the mean sea level pressure trough. Further northwest the convergence forms what is known as the Congo Air Boundary (CAB), separating Atlantic Ocean from Indian Ocean air masses. At 1000 hPa the RCM clearly shows the observed ITCZ and CAB, including cyclonic circulation over Zambia. These features are completely lacking in the FSUSM 1000 hPa circulation. In fact the only convergence observed in figure 8c is in the extreme northwest. The FSUSM 1000 hPa anticyclonic rotation over the southeast does not appear in the observed analysis.

Both exp3 and the observed field feature cyclonic circulation over Zambia at 850 hPa (Fig. 8d, e). The RCM resolves northwesterlies north of the rotation, which is missing on the ECMWF 2.5° analysis. The prominent ridge over the southeast with southeasterly on-shore winds simulated by the FSUSM is a somewhat better representation of the observed 850 hPa circulation than the corresponding RCM field. The CAB convergence zone over the northern portion of the domain is displaced to the west by both the RCM and FSUSM.

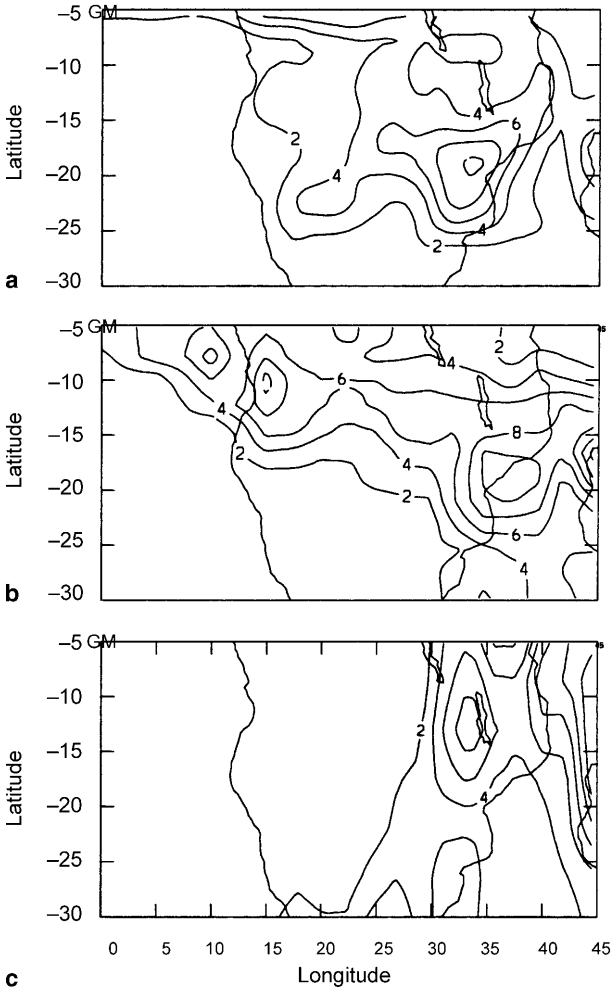

Fig. 9. February 1983 precipitation rates (mm day^{-1}). **a** exp3, **b** observed CMAP (courtesy CPC, NOAA), **c** FSUSM. Data for exp3 are represented at 0.5° grid elements, for CMAP, at 2.5° grid elements and for FSUSM, at 3° grid elements

4.2.2 Precipitation distribution

Figure 9 shows distributions of accumulated RCM exp3, FSUSM and observed rainfall for February 1983. Note that the axis of ITCZ maximum values has shifted southward compared to December 1982 (Fig. 5) in both the observed and RCM-simulated fields. The observed ITCZ rainfall maximum is oriented southeast-northwest from Mozambique to Zambia and the exp3 simulated axis is displaced slightly to the southwest. This is consistent with a similar displacement of the simulated lower tropospheric convergence zones shown in Fig. 8a. The RCM (Fig. 9a) locates a maximum over Mozambique/ Zimbabwe, displaced slightly westward of the observed location (Fig. 9b), but the displacement of the maximum by the FSUSM is much greater (Fig. 9c). In contrast to the RCM, however, the FSUSM did correctly organize the ITCZ maximum west of Lake Malawi. Over the high topography of Namibia the RCM (Fig. 9a) shows a local maximum that is not observed. Over Angola on the other hand, the CMAP analysis indicates a second maximum which is somewhat underestimated by the RCM in exp3.

4.2.3 Area averaged precipitation

We next compare area averaged rainfall for RCM and FSUSM simulations against observations. In Fig. 10, rainfall over the CAB/ITCZ zone is represented by averages between latitudes 10–20° S. The zone was further divided into three divisions: west, 10–20° E, central, 20–30° E and east, 30–40° E. Precipitation rate increases from west to east for both models are confirmed by observational evidence. However, the RCM results are considerably closer to observations than the FSUSM in the western and central regions,

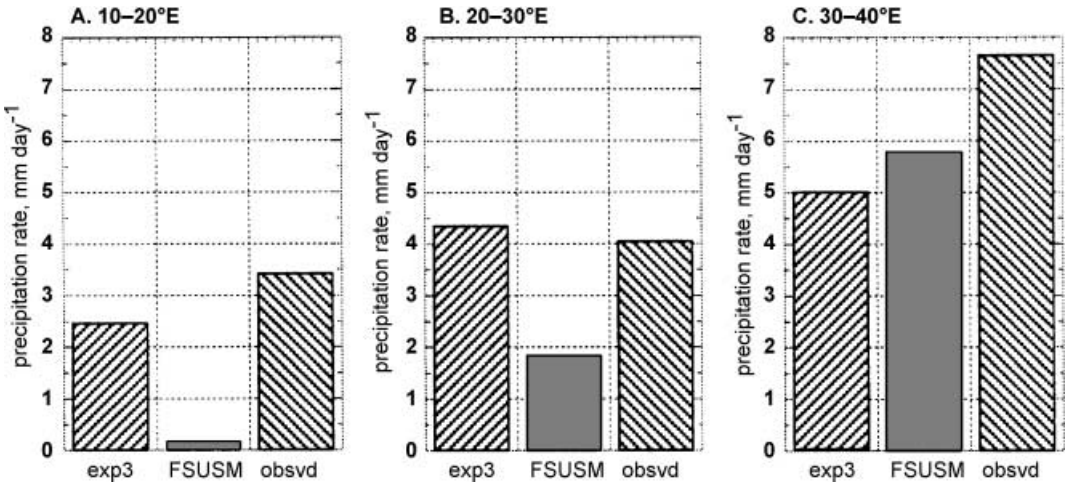

Fig. 10. Histogram of February 1983 precipitation totals (mm) averaged for each of three areas between 10–20° N over southern Africa. RCM results for exp3 are compared with FSUSM and observed CMAP (courtesy CPC, NOAA)

but not rainy enough in the east. Figure 9a shows that the unrealistic dry slot over Malawi explains this RCM insufficiency. Note that the orographic maximum over Angola is completely missed by the FSUSM. The RCM simulation indicates a somewhat weaker version of this feature, apparently exploiting the better resolved terrain relief as compared with the FSUSM which relies on the coarser 2.8° grid.

4.3 December 1988 results (exp4, exp5, exp6)

SMA for exp4 and exp6 was computed from observed NDVI shown in Fig. 1 as discussed in Sect. 2.4.

Figures 11a, c, e show RCM simulated precipitation rates for exp4, exp5 and exp6, respectively, which can be compared to observations (Fig. 11b) and the corresponding results of the FSUSM simulation (Fig. 11d). In contrast to December 1982, observed rainfall during December 1988 was heavier over Angola and Mozambique/ Zimbabwe, and the ITCZ position over Mozambique was more southerly. Exp 4 has indeed simulated heavier precipitation than for December 1982 (exp1) over Angola and Mozambique/ Zimbabwe, and its ITCZ maximum is only slightly too far north over Mozambique. Exp5, which used the original SMA formulation, simulated very unrealistically high precipitation rates over broad expanses. An explanation for this is offered in Sect. 4.4. Exp6, which was forced by ECMWF derived LBC (i.e., observational analyses), matches the observed location of the ITCZ precipitation maximum quite well, but it exaggerates rainfall rates compared to CMAP over Lake Malawi. While exp4 overestimates precipitation over southern Angola/northern Namibia, exp6 slightly underestimates it. Differences between exp4 and exp6 reflect the sensitivity of the RCM results to the LBC, and in this case study these differences are rather small, emphasizing the importance of RCM dynamics and land surface and topography effects. The FSUSM simulation shows approximately the same precipitation regime over the north for December 1982 and 1988, with appropriate increases in the latter year only over Zimbabwe. It does not produce a realistic ITCZ precipitation maximum, except over northern Angola.

Figure 12 compares RCM simulated and observed precipitation rates for December 1988 for each of the three soil types. Higher rainfall rates were evident over each subregion as compared with December 1982. The RCM slightly overestimates observed accumulations in the three subregions, but exp5 consistently gives larger errors by exaggerating rainfall rates.

4.4 Mesoscale precipitation

Giorgi et al. (1994) separated MM4 precipitation fields into large-scale (LS) and mesoscale (MS) components. Following their approach the mesoscale response is computed as the difference between a grid point value and the large-scale

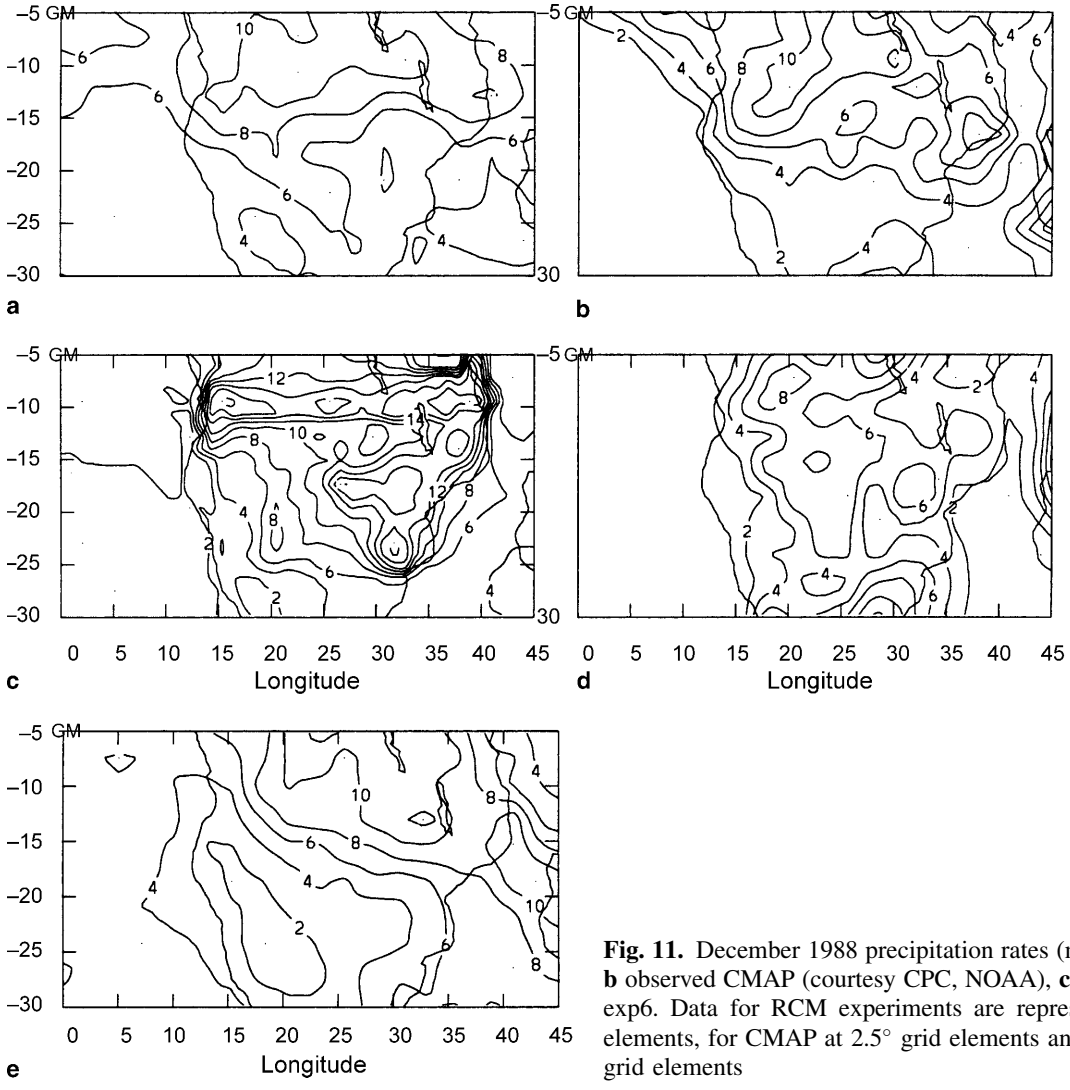

Fig. 11. December 1988 precipitation rates (mm day^{-1}). **a** exp4, **b** observed CMAP (courtesy CPC, NOAA), **c** exp5, **d** FSUSM, **e** exp6. Data for RCM experiments are represented at 0.5° grid elements, for CMAP at 2.5° grid elements and for FSUSM at 3° grid elements

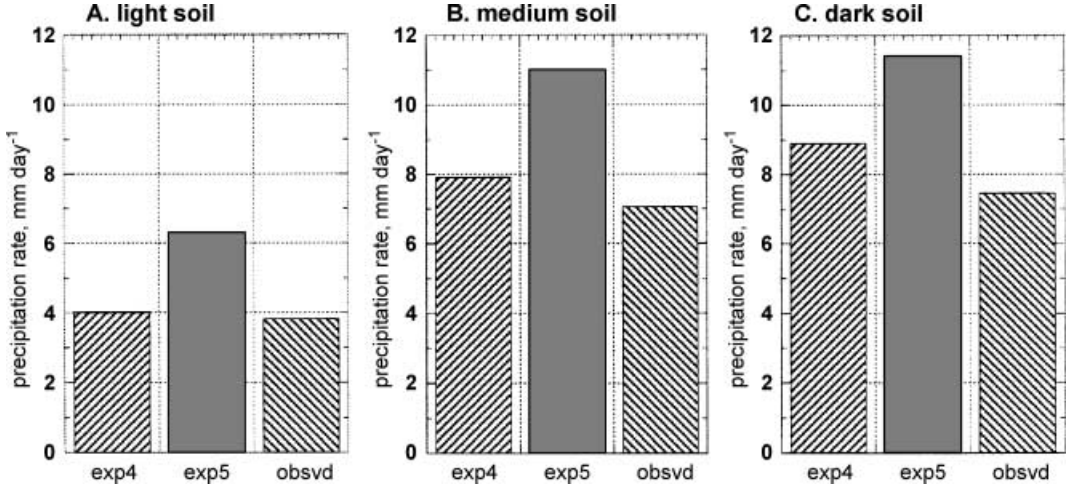

Fig. 12. Histogram of December 1988 rainfall rates averaged over each of three soil types for exp4, exp5 and observed CMAP (courtesy CPC, NOAA)

averaged data. Spatial distributions of the MS component of the RCM simulated precipitation were computed at each i-th grid element as follows:

$$MS_{\mathrm{i}} = Pr_{\mathrm{i}} - LS_{\mathrm{n}}, \tag{4}$$

where

$$LS_{\mathrm{n}} = (1/36)\Sigma Pr_{\mathrm{i}} \tag{5}$$

is the large-scale spatial average of the monthly mean RCM simulated precipitation over the n-th area of 6×6 grid elements which covers about $90 \times 10^3\,\mathrm{km}^2$. In Eq. (4) and Eq. (5), Pr_i is the RCM monthly mean precipitation rate at grid element i within the n-th area and MS_i is the mesoscale signal. *MS* accordingly is a measure of the effects of high spatial resolution forcing such as topography and land surface characteristics on the simulated precipitation field.

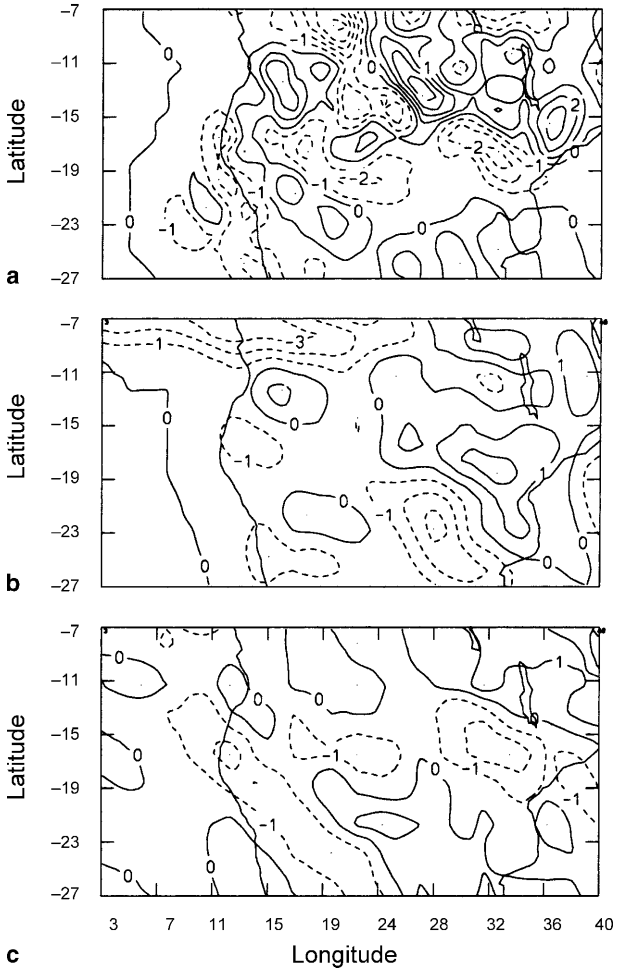

Fig. 13. RCM mesoscale component of precipitation for three simulation experiments forced by FSUSM LBC. **a** exp1, December 1982, **b** exp3, February 1983, **c** exp4, December 1988

Figure 13 illustrates the RCM mesoscale response for exp1, exp3 and exp4. During the very dry month of December 1982 (exp1, Fig. 13a) MS effects were quite prominent, emphasizing the orographic enhancement of the precipitation field and showing prominent mesoscale centers of convection within the ITCZ. Figure 13a also shows that MS maxima for this example are 2–4 mm day^{-1} interspersed with comparable minima. The MS maximum in Fig. 13b corresponds to the Mozambique precipitation maximum simulated for February 1983 (Fig. 9) and it reflects the large gradient along the southern edge of the ITCZ. The MS effect in exp4 (Fig. 13c) is considerably reduced, suggesting the dominance of large-scale influences during that month. Since the December 1988 regime was dominated by large-scale uplift, the inhibition of surface heating by the old SMA scheme was not as important to precipitation generation as during December 1982. While exp 2 underestimated local convective precipitation, exp 5 overestimated large-scale precipitation, probably because of high ambient humidities.

4.5 Vertical structure

4.5.1 Temperature profiles

The vertical thermal structure of the RCM-simulated monthly climate is validated at each standard pressure level by computing root mean square errors (RMSE) between the monthly mean RCM and spatially interpolated ECMWF (observed) temperature fields for land grid elements.

Profiles of the respective RMSE for December 1988 and December 1982 are shown in Fig. 14a, b. The RCM, utilizing SMA that is dependent on vegetation and albedo (exp1, exp4), resulted in lower RMSE temperature errors than the controls (exp2, exp5), especially below 700 hPa where land surface processes involving large inland lakes, vegetation, and topographic features influence the planetary boundary layer. Within the near-surface layer, the RMSE for the simulations that benefited from the SMA dependence on vegetation and albedo are lower by 2–3 K.

Figure 14b shows three profiles of RMSE for December 1988, namely: a profile for exp4

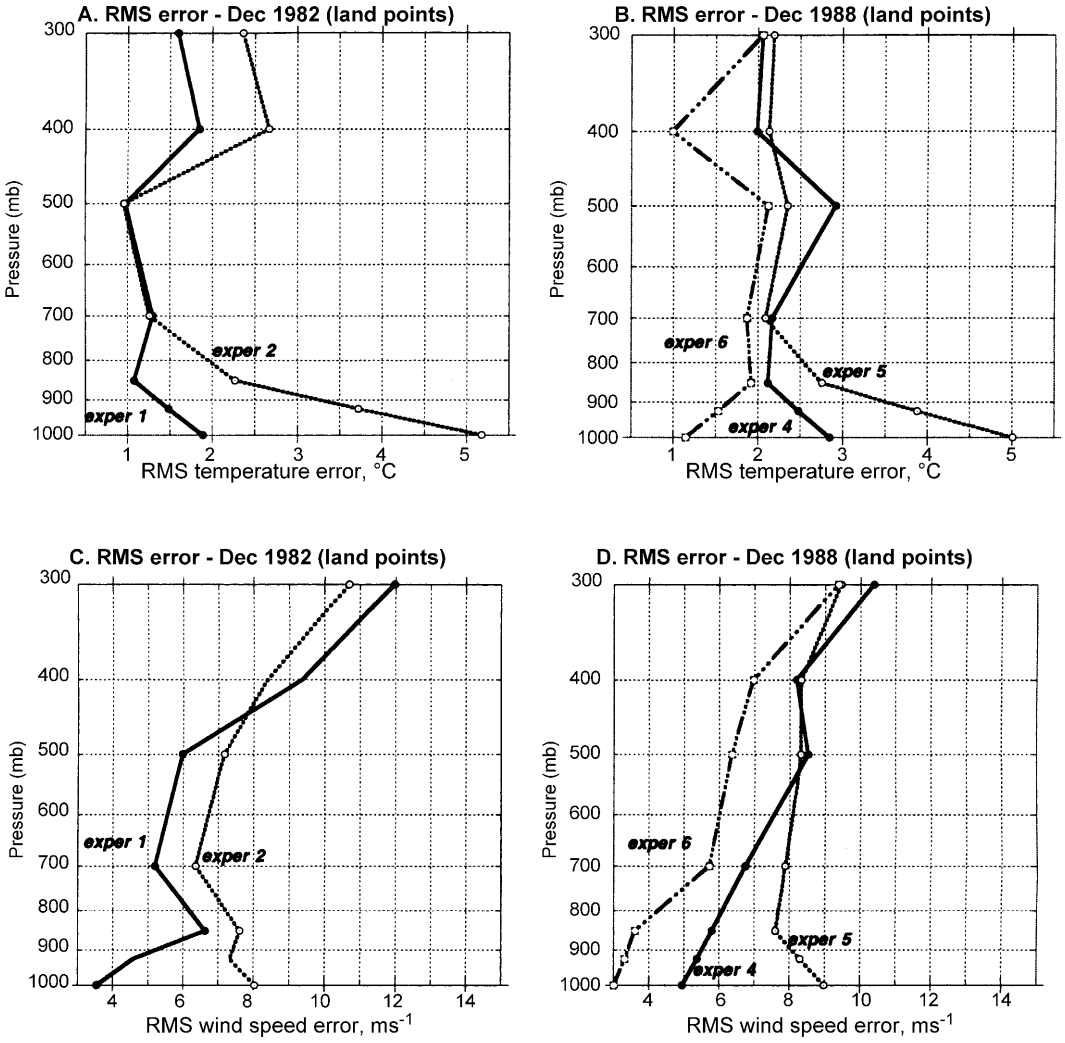

Fig. 14. Simulated profiles of root-mean-square errors of monthly mean temperature and wind speed (over land elements) for the five December simulation experiments. **a** temperature, December 1982; **b** temperature, December 1988; **c** wind speed, December 1982; **d** wind speed, December 1988

(FSUSM LBC), its control (exp5), and exp6 which used LBC from ECMWF analyses. The performance of the RCM in the three experiments differs significantly in the lower troposphere. RMSE for Exp6, forced by observational analyses, are almost 2° K lower than for exp4, which was forced by the FSUSM LBC. Since both computed SMA with vegetation and albedo dependence, the difference in the skill can be attributed to the use of observed rather than model data for LBC. Another point worthy of note is that exp6 RMSE at all levels are the lowest from among the three experiments shown in Fig. 14b, but using LBC from the global model causes only a slight deterioration of results. This is most evident in the mid- troposphere where RMSE of exp4 and exp6 are comparable.

4.5.2 Wind speed profiles

The wind speed RMSE for December 1982 and 1988 are shown in graphs 14c and 14d, respectively. The biggest differences in RCM simulated wind speeds between the experiments also occur in the lower troposphere. Application of the SMA scheme that is dependent on NDVI and albedo (exp1, exp4) reduces the RMSE by about $4\,ms^{-1}$ near the surface, and by $1–2\,ms^{-1}$ between 850 and 700 hPa. As with temperature, SMA has less of an impact in the middle and

upper troposphere. RMSE for exp6 which benefited from observed LBC (ECMWF) are quite low, within the lower troposphere some $2\,ms^{-1}$ lower than when FSUSM LBC are used.

5. Discussion and conclusions

The paper discusses month long climate simulations over southern Africa by the CCSR/GISS regional climate model (RCM) on a grid with a 0.5° spacing. In particular, we have demonstrated an improvement in monthly simulated climate over southern Africa resulting from the application of multivariate soil moisture prediction functions that account for soil type, vegetation and albedo in addition to rainfall and terrain relief. This alternative to a full-blown physical model has the advantage of simplicity and computational efficiency.

The RCM's predecessor, the FSU RCM, used a soil moisture availability (SMA) scheme which, although sensitive to terrain relief, was nevertheless a single function developed from India climate data over all land surface types. The algorithm was useful for short integrations as an improvement over the previous approach which prescribed time invariant SMA distributions. The SMA scheme described here is more suitable for longer (climate) simulations of a month or more since it accounts for soil type, vegetation cover and albedo. Simulations of the monthly mean climate over southern Africa with the new scheme were compared to control runs using the former model and the impact was analyzed. Additional comparisons were made to FSU global spectral model (FSUSM) simulations at 2.8°, CPC Merged Analyses of Precipitation at 2.5° and to ECMWF observational analyses also at 2.5°.

In all, six monthly RCM climate simulations over southern Africa were evaluated. All but one of the RCM runs were driven with FSUSM simulation data as the LBCs, while the sixth used ECMWF observational data sets. All simulations relied on observed SST. Results demonstrated that the RCM-simulated monthly climate is more realistic when the parameterized formulation for SMA includes information about land surface characteristics of the region under study.

In the simulation for December 1982, the new scheme caused a significant reduction in SMA which in turn decreased evapotranspiration. Compared to the control simulation, the drier land surfaces allowed more realistic surface latent and sensible heat fluxes which had the effect of increasing the diurnal range of the ground temperature. The abbreviated diurnal cycle in the control apparently inhibited thermal convection to the extent that heavy rain was unrealistically confined to the windward slopes of high terrain, compared to the new version which achieved a spatial distribution of rainfall that was much closer to observational evidence. In the simulation for December 1988, the new SMA scheme reduced unrealistically excessive control run precipitation, thereby demonstrating that beneficial impacts of the modification can operate in either direction.

The seasonal evolution of climate over southern Africa was captured by the RCM February 1983 experiment which in effect downscaled a continuous FSUSM simulation. In particular, the southerly migration of the ITCZ precipitation maximum was successfully represented by the RCM in significant contrast to the global model's corresponding configuration. These results demonstrate that the dynamic downscaling with the RCM is not merely a spatial interpolation of the coarse grid results. The RCM exploits its higher resolution to better resolve variable gradients and topographic influences.

An example of interannual climate variability compared December simulations for 1982 and 1988. Both the older and newer versions of the RCM simulated widespread increases in precipitation between these two years, and increases were indeed observed. However, the magnitudes of 1988 versus 1982 differences were overall much more realistic when based on the more sophisticated SMA scheme. The former modeling scheme gave 1988 minus 1982 differences that were some 3–4 times the observed values with little spatial correlation to the observed difference field. However, even with the latest model, discrepancies between the simulated and observed positions of the ITCZ (from Mozambique to Zambia) resulted in some displacements of RCM interannual rainfall difference centers. Errors in RCM simulated temperature and wind profiles for these two Decembers were consistently smaller using the newer RCM, and the positive impacts, which were largest near the ground, remained evident at least up to 700 hPa.

When LBCs are provided from ECMWF analyses in lieu of model predicted fields, information about the actual climate is introduced into the RCM domain, contributing to a more realistic simulation. Comparison of the ECMWF-forced simulation with the parallel FSUSM-forced run showed discernable, but surprisingly small improvements in the spatial distribution of precipitation. The impact on vertical profiles of temperature and wind speed errors was more impressive, perhaps in part because ECMWF data were used for the validation of those variables. Overall, the benefits of simulations at the high resolution of the RCM (0.5° grid) likely compensate for errors introduced by modeled, as opposed to observed, lateral boundary climate information. These results suggest that nesting the RCM within GCM extended-range climate predictions has definite potential for providing skillful predictions of local climate.

An analysis of the mesoscale component of RCM precipitation simulations showed different patterns for each of the three case studies. It emphasized the importance of mesoscale convective centers within the ITCZ and orography during December 1982 in contrast with the much weaker mesoscale signal during the overall rainier December 1988. This means that mesoscale influences were dominant during the dry month while large scale precipitation dominated during the rainier month. Positive rainfall anomalies in the region are associated with large-scale mechanisms, such as the Walker circulation, which exert a more spatially uniform influence on the precipitation regime in southern Africa. In the absence of such favorable large-scale dynamics, local influences apparently play a greater role. The more crude estimates of SMA exaggerated ground moisture thereby inhibiting ground heating and local convective precipitation during the drier month. During the rainier month this version caused excessive and widespread precipitation due the combination of high humidities and large scale uplift.

More simulations are required to better evaluate the model's potential and in order to tune it to improve skill. Simulations over South America currently being evaluated suggest that the new SMA approach is easily adaptable to other regions. Ultimately, the RCM's most important application will be in making seasonal climate predictions for selected regions.

Acknowledgements

This research was supported by the National Science Foundation under grants nos. ATM 97-25142, ATM 00-89563 and by the NASA Climate and Earth Observing System Programs.

References

Anthes RA (1977) A cumulus parameterizing scheme utilizing a one-dimensional cloud model. Mon Wea Rev 105: 270–286

Anthes RA, Kuo YH, Hsie EY, Low-Nam S, Bettge TW (1989) Estimation of skill and uncertainty in regional numerical model. Quart J Roy Meteor Soc 115: 763–806

Arakawa A, Lamb VR (1977) Computational design of the basic dynamical processes of the UCLA general circulation model. Meth Comput Phys 17: 174–265, Acadic Press, 377 pp

Bounoua L (1992) Land surface processes and climate modeling. PhD Diss, Dept. of Meteorol., The Florida State University, 196 pp

Budyko MI (1986) The evolution of the biosphere. D. Reidel, Dordrecht: Holland, 423 pp

Chang LW (1978) Determination of surface flux of sensible heat, latent heat and momentum utilizing the bulk Richardson number. Papers in Meteor Res 1: 16–24

Chen JH, Miyakoda K (1974) A nested grid computation for the barotropic free surface atmosphere. Mon Wea Rev 102: 181–190

Dastoor A, Krishnamurti TN (1991) Landfall and structure of a tropical cyclone: Sensitivity of the model predictions to soil moisture parameterization. Bound Layer Meteorol 55: 345–380

Davenport ML, Nicholson SE (1993) On the relation between rainfall and the Normalized Difference Vegetation Index for diverse vegetation types in East Africa. Int J Remote Sensing 14: 2369–2389

Davies HC (1983) Limitation of some common lateral boundary schemes used in regional NWP models. Mon Wea Rev 111: 1002–1112

Deardoff J (1978) Efficient prediction of ground surface temperature and moisture with inclusion of a layer of vegetation. JGR 83: 1889–1903

Dickinson RE, Henderson-Sellers A, Kennedy PJ, Wilson MF (1986) Biosphere-atmosphere transfer scheme (BATS) for the NCAR-community climate model. NCAR Tech Note, TN275 + STR, 69 pp

Druyan L, Fulakeza M, Thiaw W (2000) Regional model simulations of African wave disturbances. J Geophys Res 105: 7231–7255

Druyan L, Fulakeza M, Lonergan P, Saloum M (2001) A regional model study of synoptic features over West Africa. Mon Wea Rev 129: 1564–1577

Fulakeza MB (1991) Impact of sea surface temperature anomalies on eastern Africa climate. M. S. thesis, The Florida State University, Tallahassee, FL, 92 pp

Fulakeza M (1998) Modeling regional climate of southern Central Africa, PhD diss, Dept. of Meteorol., Florida State University, Tallahassee, FL, 243 pp

Gash JH, Wallace JS, Lloyd CR, Sivakumar MVK, Renard C (1991) Measurements of evaporation from fallow Sahelien Savannah at start of dry season. Quart J Roy Meteor Soc 117: 716–749

Giorgi F, Bates GT (1989) The climatological skill of a regional model over complex terrain. Mon Wea Rev 117: 2325–2347

Giorgi F (1990) Simulation of regional climate using a limited area model nested in a general circulation model. J Climate 3: 941–963

Giorgi F (1991) Sensitivity of simulated summertime precipitation over the western United States to different physics parameterizations. Mon Wea Rev 119: 2870–2888

Giorgi F, Bates GT, Nian S (1993) The multi-year surface climatology of a regional atmospheric model over western United States. Mon Wea Rev 121: 2794–2813

Giorgi F, Hostetler SW, Brodeur CS (1994) Analysis of the hydrology in regional climate model. Quart J Roy Meteorol Soc 20: 161–183

Giorgi F, Marinucci (1996) An investigation of the sensitivity of simulated precipitation to model resolution and its implication for climate studies. Mon Wea Rev 124: 148–166

Giorgi F, Mearns L (1999) Introduction to special section: Regional climate modeling revisited. J Geophys Res 104: 6335–6352

Justice CO, Townshend JRG, Holben BN, Tucker CJ (1985) Analysis of the phenology of global vegetation using meteorological satellite data. Int J Remote Sensing 6: 1271–1318

Kanamitsu M (1975) On numerical prediction over a global tropical belt. Rep. No. 75-1, Dept. of Meteorol. Florida State University, Tallahassee, FL, 142 pp

Kondratyev K (1972) Radiation processes in the atmosphere. WMO Pub. #309, World Meteorological Organization, Geneva

Krishnamurti TN, Low-Nam S, Pasch R (1983) Cumulus parameterization and rainfall rates II. Mon Wea Rev 111: 815–828

Krishnamurti TN, Oosterhof D, Dignon N (1989) Hurricane prediction with a high resolution global model. Mon Wea Rev 116: 631–669

Krishnamurti TN, Kumar A, Yap KS, Dastoor AP, Davidson N, Sheng J (1990) Performance of high resolution mesoscale tropical prediction model. Adv Geophys (Dmowska R, Saltzman B, eds) 32: 133–286

Krishnamurti TN, Rohaly G, Oosterhof D (1994) A note on the simulation of winter monsoon anomalies during an El Niño year. Meteorol Atmos Phys 53: 51–59

Krishnamurti TN, Bedi HS, Rohaly G, Fulakeza MB, Oosterhof D, Ingles K (1995) Seasonal monsoon forecast for the years 1987 and 1988. Global Planetary Change 10: 79–95

Kumar A (1989) A documentation of the FSU limited area model. Rep. No. 89-4, Dept. of Meteorol., Florida State University, Tallahassee, FL, 301 pp

Kuo HL (1965) On the formation and intensification of tropical cyclone through latent heat release by cumulus convection. J Atmos Sci 22: 40–63

Kuo H (1974) Further studies of the parameterization of the influence of cumulus convection on large-scale flow. J Atmos Sci 31: 1232–1240

Lare AR (1992) An investigation into land surface feedback and the African drought using climatonomy modeling. PhD Diss, The Florida State University, Tallahassee, FL, 320 pp

Leslie LM, Mills GA, Gauntlett D (1981) The impact of FGGE data coverage and improved numerical techniques in numerical weather prediction in the Australian region. QJR Meteorol Soc 107: 629–642

Malo AR, Nicholson SE (1990) A study of rainfall and vegetation dynamics in the African Sahel using normalized difference vegetation index. J Arid Envir 19: 1–24

Mintz Y (1984) The sensitivity of numerically simulated climates to land surface boundary conditions. In: The Global Climate (Houghton, TJ, ed), Cambridge University Press, 79–105

Miyakoda K, Roasati A (1977) One way nested grid models. The interface conditions and numerical accuracy. Mon Wea Rev 105: 1092–1107

Nicholson SE, Davenport ML, Malo AR (1990) A comparison of the vegetation response to rainfall in the Sahel and East Africa, using Normalized Difference Vegetation Index from NOAA AVHRR. Climatic Change 17: 209–241

Ogallo LJ (1987) Impacts of the 1982–83 ENSO event on Eastern and Southern Africa. The societal impacts associated with the 1982–83 worldwide climate anomalies, Environmental and Societal Impacts Group, NCAR/UNEP, 105 pp

Posey JW, Clapp PF (1964) Global distribution of normal surface albedo. Geophys Int 4: 33–48

Reynolds R, Smith T (1994) Improved global SST analyses. J Climate 7: 929–948

Rosenzweig C, Abramopoulos F (1997) Land-surface model development for the GISS GCM. J Climate 10: 2040–2054

Sellers PJ, Mintz Y, Sud YC, Dalcher A (1986) A simple biosphere model (SiB) for use within general circulation models. J Atmos Sci 43: 505–531

Sellers PJ, Dorman JL (1987) Testing simple biosphere model (SiB) using point micrometeorological and biophysical data. J Climate Appl Meteorol 26: 622–651

Sun L, Semazzi F, Giorgi F, Ogallo L (1999a) Application of the NCAR regional climate model to eastern Africa. 1. Simulation of the short rains of 1988. J Geophys Res 104: 6529–6548

Sun L, Semazzi F, Giorgi F, Ogallo L (1999b) Application of the NCAR regional climate model to eastern Africa. 2. Simulation of interannual variability of short rains, J Geophys Res 104: 6549–6562

Tiedtke M (1984) The sensitivity of the time mean large scale flow to cumulus convection in ECMWF model.

Workshop on convection in large scale numerical models, ECMWF, 28 Nov–1 Dec, 1983, 297–317

Torrance J (1972) Malawi, Rhodesia and Zambia. In: Climates of Africa (Griffiths, ed) Elsevier, Amsterdam, pp 409–460

Tucker C, Sellers P (1986) Satellite remote sensing of primary production. Int J Remote Sensing 7: 1395–1416

Wilson MF, Henderson-Sellers A (1985) A global archive of land cover and soils data for use in general circulation climate models. J Climatology 5: 119–143

Xie P, Arkin P (1997) Global precipitation: a 17-year monthly analysis based on gauge observations, satellite estimates and numerical outputs, Bull AMS 78: 2539–2558

Author's addresses: M. Fulakeza, Center for Climate Systems Research, Columbia University at the NASA/ Goddard Institute for Space Studies New York, USA; T. N. Krishnamurti, Department of Meteorology, Florida State University, Tallahassee, USA

Verleger: Springer-Verlag KG, Sachsenplatz 4–6, A-1201 Wien. – Herausgeber: Prof. Dr. Reinhold Steinacker, Institut für Meteorologie und Geophysik, Universität Wien, Silbergasse 45, A-1190 Wien. – Redaktion: Innrain 52, A-6020 Innsbruck. – Satz und Umbruch: Thomson Press (India) Ltd., Chennai. – Druck und Bindung: Grasl Druck&Neue Medien, A-2540 Bad Vöslau. – Verlagsort: Wien. – Herstellungsort: Bad Vöslau. – Printed in Austria.

Offenlegung gemäß § 25 Abs. 1 bis 3 Mediengesetz:
Unternehmensgegenstand: Verlag von wissenschaftlichen Büchern und Zeitschriften. An der Springer-Verlag KG ist beteiligt: Springer-Verlag GmbH & Co KG, Heidelberger Platz 3, D-14197 Berlin, als Kommanditist zu 74,04%. Geschäftsführer: Rudolf Siegle, Sachsenplatz 4–6, A-1201 Wien.